Powering Fuel Cells with CO via Aqueous Polyoxometalates and Gold Catalysts

Won Bae Kim *et al.*

Science **305**, 1280 (2004);
DOI: 10.1126/science.1100860

Science (print ISSN 0036-8075; online ISSN 1095-9203) is published weekly, except the last week in December, by the American Association for the Advancement of Science, 1200 New York Avenue NW, Washington, DC 20005.

the Lake Tahoe sequence is most likely in response to rock failure due to a high strain rate, typical of dike injection (*7*). The injection front of a propagating dike is reflected by the temporal progression of earthquake depths, whereas the high-frequency character of the events requires brittle failure of rock at the crack tip. Also, tensile failure along east-dipping structures would be consistent with east-west extension along the Great Basin Sierra Nevada transition near Lake Tahoe. High dilatational strain rates are inferred from GPS data in the Lake Tahoe region (Fig. 4). SLID deformation and the character of the earthquake swarm are consistent with magma injection. The volumetric source required to fit SLID observations would correspond to a ~1-m-thick dike over the area of the imaged structure at depth. Dipping eastward at 50°, the lower-crustal structure would project to the surface west of the Sierra Nevada Great Basin frontal fault system west of Lake Tahoe. However, if a Sierra Nevada/Great Basin–bounding structure, or structural zone, shallows eastward into the lower crust, the event may have taken place near or within this structural boundary.

Periodic aseismic transient deformation in the Cascadia subduction zone is associated with deep-crustal LP earthquakes (25 to 45 km in depth) with tremor-like seismic signatures (*20*, *21*). Outside of subduction regions, however, deep brittle–failure earthquakes are uncommon because of the predominance of a brittle-ductile transition in the mid-crust and increased temperature with depth. Brittle failure at these depths requires localized high strain rates that can result from magma injection. Deep earthquakes observed in the western Sierra Nevada foothills (*22*) may be in response to the same mechanism (Fig. 4). We suggest that this magmatic phenomenon should not be viewed as a likely precursor to volcanism, but rather as part of the tectonic cycle of lower-crustal evolution, perhaps providing a mechanism to sustain crustal thickness and crustal strength in zones of extension.

References and Notes

1. T. Dixon, M. Miller, F. Farina, H. Wang, D. Johnson, *Tectonics* **19**, 1 (2000).
2. R. Bennett, B. Wernicke, N. Niemi, A. Friedrich, J. Davis, *Tectonics* **22**, 1008.10.1029/2001TC001355 (2003).
3. C. Henry, J. Faulds, abstract presented at the EarthScope/NSF Great Basin Symposium, Lake Tahoe, California, 21 to 23 June 2004.
4. R. Schweickert, M. Lahren, K. Smith, J. Howle, *Tectonophysics*, in press.
5. S. Wesnousky, C. Jones, *Geology* **22**, 1031 (1994).
6. Nevada Seismological Laboratory Historical Earthquake Catalog, accessible and searchable at www.seismo.unr.edu/Catalog/catalog-search.html.
7. A. Rubin, D. Pollard, *Geology* **16**, 413 (1988).
8. M. Ukawa, H. Tsukahara, *Tectonophysics* **253**, 285 (1996).
9. S. R. McNutt, *International Handbook of Earthquake and Engineering Seismology, Part* A (Academic Press, Amsterdam, Netherlands, 2002), pp. 383–406.
10. V. Zobin, *Introduction to Volcanic Seismology* (Elsevier, Amsterdam, Netherlands, 2003).
11. S. Wiemer, S. McNutt, M. Wyss, *Geophys. J. Int.* **134**, 409 (1998).
12. G. Ichinose, J. Anderson, K. Smith, Y. Zeng, *Bull. Seism. Soc. Am.* **93**, 61 (2003).
13. B. Wernicke, A. Friedrich, N. Niemi, R. Bennett, J. L. Davis, *GSA Today* **10**, 1 (2000).
14. J. Zumberge, M. Heflin, D. Jefferson, M. Watkins, F. Webb, *J. Geophys. Res.* **102**, 5005 (1997).
15. G. Blewitt, *J. Geophys. Res.* **94**, 10187 (1989).
16. Z. Altamimi *et al.*, *Eos* **82**, 273 (2001).
17. S. Wdowinski, Y. Bock, J. Zhang, P. Fang, J. Genrich, *J. Geophys. Res.* **102**, 18057 (1997).
18. G. Blewitt, D. Lavallée, *J. Geophys. Res.* **107**, 2145, 10.1029/2001JB000570 (2002).
19. Y. Okada, *Bull. Seism. Soc. Am.* **75**, 1135 (1985).
20. H. Dragert, K. Wang, T. James, *Science* **292**, 1525 (2001).
21. G. Rogers, H. Dragert, *Science* **300**, 1942 (2003).
22. I. Wong, W. Savage, *Bull. Seism. Soc. Am.* **73**, 797 (1983).

23. The University of Nevada, Reno seismic network in northern Nevada is operated under the U.S. Geological Survey National Earthquake Hazards Reduction Program with support from the State of Nevada. The GPS data analysis was funded by the Department of Energy, Yucca Mountain Project. The BARGEN GPS network is funded by NSF and the Department of Energy, with operational support from UNAVCO, Inc. The GIPSY OASIS II software and global GPS data products were provided by the Jet Propulsion Laboratory. We thank G. Oppliger for a review of the manuscript and M. Coolbaugh for generating the regional strain map figure. Several stations in the Nevada K-12 seismic network, Storey County High School, Carson City High School, and Douglas County High School contributed phase arrival data for constraining earthquake locations in the lower-crustal swarm. We thank three anonymous reviewers for their time and effort in reviewing the manuscript.

Supporting Online Material

www.sciencemag.org/cgi/content/full/1101304/DC1
SOM Text
Figs. S1 to S4
References

9 June 2004; accepted 28 July 2004
Published online 5 August 2004;
10.1126/science.1101304
Include this information when citing this paper.

Powering Fuel Cells with CO via Aqueous Polyoxometalates and Gold Catalysts

Won Bae Kim, T. Voitl, G. J. Rodriguez-Rivera, J. A. Dumesic*

Electricity was produced by catalytic oxidation of carbon monoxide (CO) by using gold catalysts at room temperature. The observed rates are faster than conventional processes operating at 500 kelvin or higher for the conversion of CO with water to produce hydrogen and carbon dioxide through the water-gas shift (WGS). By eliminating the WGS reaction, we remove the need to transport and vaporize liquid water in the production of energy for portable applications. This process can use CO-containing gas streams from the catalytic reforming of hydrocarbons to produce an aqueous solution of reduced polyoxometalate compounds that can be used to generate power. The reduced polyoxometalate can be reoxidized in fuel cells that contain simple carbon anodes.

The production of H_2 for fuel cells typically involves the initial formation of a mixture of H_2, CO, and CO_2 from hydrocarbons or oxygenated hydrocarbons (*1*–*5*), followed by the water-gas shift (WGS) reaction ($CO + H_2O \rightarrow CO_2 + H_2$) to achieve the high conversions of CO to CO_2 (*6*–*9*) necessary for proton-exchange membrane (PEM) fuel cells, in view of the strong poisoning effects of CO on Pt-based anodes (*10*). The WGS reaction represents a major bottleneck in the production of H_2 because this exothermic reaction is slow at the low temperatures (~500 K) required to achieve favorable equilibrium conversions. In addition, the WGS reaction imposes an important limitation for the production of H_2 for portable applications because large amounts of liquid water must be transported and vaporized. Here, we demonstrate a process that bypasses the WGS reaction during the production of fuel-cell-grade H_2 by using the CO directly as an additional source of energy from H_2 streams. This process is especially promising for the production of electrical energy from renewable biomass-derived oxygenated hydrocarbons because these reactants have C:O stoichiometric ratios equal to 1:1, and they therefore generate H_2 and CO in nearly equal amounts during catalytic decomposition.

Our process for oxidation and use of CO involves the reaction of CO and liquid water with a reducible polyoxometalate (POM) compound, such as $H_3PMo_{12}O_{40}$, that serves as a strong oxidizing agent for CO and as an energy-storage agent for electrons and protons, over gold nanotubes or nanoparticles, and it takes advantage of the high catalytic activities of gold nanoparticles for CO oxidation (*11*–*13*), especially in the presence of liquid water (*14*, *15*). This catalytic process

Department of Chemical and Biological Engineering, University of Wisconsin, Madison, WI 53706, USA.

*To whom correspondence should be addressed. E-mail: dumesic@engr.wisc.edu

can be accomplished at room temperature, whereas the WGS reaction must be operated at elevated temperatures (at least 400 K and typically above 500 K) (*6*, *16*). In our process, CO is removed from the gas stream by oxidizing it to CO_2, thereby forming an aqueous solution of reduced POM species according to the following representative reaction:

$$CO_{(g)} + H_2O_{(l)} + PMo_{12}O_{40}^{3-}{}_{(aq)} \rightarrow$$

$$CO_{2(g)} + 2H^{+}{}_{(aq)} + PMo_{12}O_{40}^{5-}{}_{(aq)}$$

This solution contains stored energy in the form of protons and electrons associated with reduced metal cations that can be reoxidized readily at a fuel-cell anode by the transfer of electrons from the POM to the electrode and the transport of protons through the PEM to the cathode. Accordingly, this process for CO oxidation not only removes CO from gas streams for fuel cells, but also converts the energy content of CO into a liquid that can subsequently be used to power a fuel cell. Thus, whereas previous studies of CO oxidation have used irreversible oxidizing agents such as O_2 (*17*, *18*), our process uses aqueous-phase POM compounds that undergo reversible oxidation-reduction reactions. In this way, the reducible POM compound facilitates the CO removal step by undergoing reduction, and the reduced POM then serves as a fuel for the electrical energy generation step by undergoing oxidation at a fuel-cell anode. Thus, the use of the POM species as redox shuttle eliminates the need to convert CO with H_2O to gaseous H_2 and CO_2 as an intermediate reaction for power generation.

To illustrate a possible application of our process for CO use, we consider ethylene glycol as a fuel source, which decomposes according to the stoichiometric reaction

$$C_2O_2H_{6(l)} \longrightarrow 2CO_{(g)} + 3H_{2(g)}$$

This reaction can be carried out by using a supported catalyst (for example, 3 weight percent Pt/Al_2O_3) with CO and H_2 selectivities of 90% or greater with 50% conversion of ethylene glycol at the temperatures near 500 K. Ethylene glycol dissociation is endothermic (234 kJ mol^{-1}) and requires combustion of 0.83 moles of CO for an energetically neutral process to produce 3 moles of H_2 and 1.17 moles of CO for energy production. If the H_2 and CO are separated, then the H_2 can be sent to a PEM fuel cell operating at 50% efficiency, 0.83 moles of CO can be combusted, and the remaining 1.17 moles of CO can be converted to electrical energy at 0.35 V (corresponding to ~25% of the standard Gibbs free-energy change for CO combustion). The overall efficiency for production of energy from the ethylene glycol fuel by this process is equal to 40%. This process does not require the use of water, as would be needed for ethylene glycol reforming (*2*, *3*).

$$C_2O_2H_{6(l)} + 2H_2O_{(l)} \longrightarrow 2CO_{2(g)} + 5H_{2(g)}$$

In this respect, the energy content of liquid ethylene glycol is about 20 kJ cm^{-3} (equal to 60% of the value for octane), whereas the energy content of a stoichiometric liquid mixture of ethylene glycol and water is about 10 kJ cm^{-3}. In contrast, the energy density of H_2 at a pressure of 690 bar (~10,000 psi) is only equal to about 7.5 kJ cm^{-3}. Moreover, the ethylene glycol fuel is nonflammable and can be stored safely.

Figure 1 shows a schematic representation of the reactor system used to study the reduction of aqueous solutions of POM compounds by CO in a gold nanotube membrane reactor and the subsequent generation of electrical energy from these reduced POM solutions that contain protons in the aqueous phase and electrons associated with the POM. Most of our studies were carried out using aqueous solutions of $H_3PMo_{12}O_{40}$ [which has the Keggin structure comprised of tetrahedral PO_4 surrounded by 12 octahedral MoO_6 (*19*)] as the POM oxidizing agent, which is yellow in color and stable at temperatures up to 473 K in solid form. Reaction with CO over the gold catalyst leads to the formation of CO_2 and an aqueous solution that has the characteristic deep blue color that is caused by charge transfer between Mo^{5+} and neighboring Mo^{6+} species (*20*). The reduction of $H_3PMo_{12}O_{40}$ by CO does not take place at room temperature without the gold catalyst. This aqueous solution containing reduced POM species was delivered to a fuel cell constructed with an anode fashioned from a gold nanotube membrane or made from a simple carbonlike graphite without any precious metal. The cathode of the fuel cell was comprised of Pt supported on carbon for cases in which O_2 was used as the oxidizing agent (the upper fuel cell system in Fig. 1). For cases in which the oxidizing agent was an aqueous solution of $H_3PMo_{12}O_{40}$, the cathode was composed of a gold nanotube membrane or made from carbon (the lower fuel cell system in the figure). The latter case is a completely precious metal–free fuel-cell system. Oxidation of the reduced POM solution at anode does not require a precious-metal electrode because the protons and electrons have already been separated during the CO oxidation step over the gold catalyst.

The rate of CO_2 production (Fig. 2) with aqueous solutions of POM compounds on gold nanotube membranes increases with the concentration of the aqueous POM solution up to 0.05 M, and the rate is first order with respect to the partial pressure of CO in the gas stream. [Images of gold nanotubes from scanning electron microscopy are presented

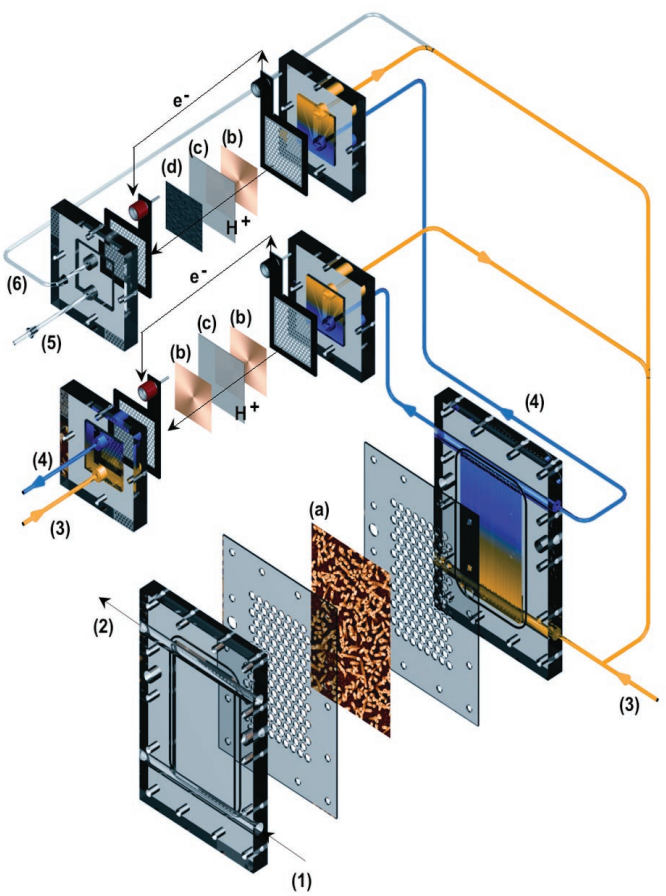

Fig. 1. Schematic diagram of the membrane reactor coupled with fuel cells to study CO oxidation at the membrane reactor and energy transfer at the fuel cells. (1) CO inlet, (2) CO_2 outlet, (3) oxidized POM inlet, (4) reduced POM outlet from membrane reactor and from fuel cell cathode or inlet to the fuel cell anodes, (5) O_2 inlet, (6) H_2O outlet, (a) gold nanotube membrane catalyst after RIE for the interface of CO gas and liquid POM solution, (b) electrodes fashioned from a simple carbon or gold nanotube membrane with surface gold, (c) Nafion PEM, and (d) cathode made of Pt/C.

in fig. S1 (*21*).] The rate is enhanced when the gold nanotubes within the track-etched pores of polycarbonate template were exposed from the polycarbonate to a depth of 1 to 2 μm by selectively etching the membrane using reactive ion etching (RIE) with an O_2 plasma (*22*). The rate of CO oxidation per gram of gold is greater for membranes containing smaller amounts of gold because the average particle size of gold is smaller for these materials (fig. S1), thus leading to higher surface areas per gram of gold. This result suggests that the rate of CO oxidation can be altered by changing the morphology of the gold catalyst, for example, by changing the inner and/or outer pore diameters of the gold nanotubes.

Catalysts consisting of gold nanoparticles on various supports should be promising candidates for achieving high rates of CO oxidation by aqueous solutions of POM compounds, because these catalysts have been shown to exhibit high rates of CO oxidation by O_2 (*17*, *18*) or by H_2O (*6*, *23*) at low temperatures. Indeed, we have observed very high rates of CO oxidation by aqueous solutions of $H_3PMo_{12}O_{40}$ over nanoparticles of gold supported on carbon or titania with gold catalysts provided by the World Gold Council (sample 4D or 18A, respectively) (fig. S2). Typically, these experiments were carried out at 298 K in a pressurized batch reactor at a CO pressure of 15 bar with 20 cm^3 of 0.05 M POM solution. The rate of CO_2 production at low conversions was approximately 16×10^4 μmol gAu^{-1} min^{-1} (~3500 cm^3 at 273 K and 1 bar of gaseous CO_2 produced per gram of gold per minute), which is equivalent to a turnover frequency (TOF) of 4.3 s^{-1}, assuming a gold dispersion of 12% based on the average diameter of the gold particles (7 to 10 nm) on carbon. This high specific rate achieved even at room temperature is comparable to or even faster than rates of CO oxidation by O_2 over supported gold catalysts at 353 K (30×10^4 μmol gAu^{-1} min^{-1}) (*24*) and rates of WGS over cyanide-leached gold catalysts at 523 K (3.7×10^4 μmol gAu^{-1} min^{-1}) (*6*). The rate of CO_2 production and TOF are very high at pressures near 1 bar (equal to 3×10^4 μmol gAu^{-1} min^{-1} and 0.85 s^{-1}, respectively, as shown in fig. S2), which suggests that our room-temperature process could be applied to gaseous streams produced from a conventional catalytic reforming of hydrocarbons, without involving the WGS reaction as an intermediate step to remove CO. Moreover, we have observed that the rate of CO oxidation by our process is 10 times as fast as the rate of H_2 oxidation when both gases are passed separately over a gold catalyst, and the rate of CO oxidation is at least an order of magnitude faster than the rate of H_2 oxidation when using a $CO:H_2$ gas mixture containing 10% CO. The rate of H_2 oxidation was measured by monitoring the color change of the POM solution using an ultraviolet-visible spectrometer operating at 500 nm. These results indicate that our process can be used to effectively remove CO from H_2 gas streams for fuel-cell applications.

The highest energy density obtained in this work was 2.5 moles of CO_2 produced per liter of solution containing $H_3PMo_{12}O_{40}$ at a concentration of 1 M, corresponding to 5 electrons per Keggin unit. This extent of storage was achieved with a pressurized batch reactor containing the solution of POM compound with gold nanoparticle catalysts, operating at room temperature and a CO pressure of 15 bar. The extent of POM reduction calculated from the CO_2 production agreed within 20% with the extent of reduction measured by integrating the electrical current versus time produced when the reduced solution was completely reoxidized in a fuel cell discharged at constant resistance, and dividing this value by the Faraday constant. [See table S1 for details (*21*).] We believe that the rate of CO oxidation as well as the energy storage capacity could be improved by further studies among the large number of other POM compounds that can be synthesized (*25*).

The generation of power by using reduced POM solutions, produced from CO oxidation, is not limited to conventional electrodes (e.g., Pt based). Figure 3 shows curves of voltage versus current density from a single cell for various combinations of anodes, cathodes, and reduced POM solutions. Although higher current densities (by 20 to 50%) are achieved with electrodes containing precious metals (i.e., Pt, Au) with a Nafion (Sigma-Aldrich, St. Louis, MO, USA) PEM (*21*), it can be seen that good current densities can be generated with a simple carbon anode. Good current densities can be generated even when the Pt-containing cathode used with O_2 is replaced by a simple carbon cathode used with oxidized $H_3PMo_{12}O_{40}$.

Current H_2 PEM fuel cells operating with Pt-based electrodes have current densities higher than 100 mA cm^{-2}. However, these fuel cells have been highly optimized, and they require precious metals to oxidize H_2 at the anode and reduce O_2 at the cathode. Our

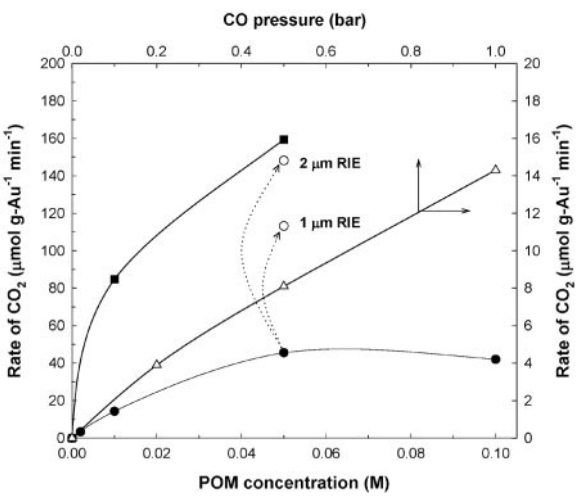

Fig. 2. Rate of CO oxidation with POM ($H_3PMo_{12}O_{40}$) on gold nanotube membranes at 298 K and a total pressure of 1 bar. Rate of CO_2 production on membrane prepared by electroless deposition of gold for 2 hours versus POM concentration (filled circles), versus CO partial pressures (M = 0.01) (open triangles), and after RIE treatment to remove 1 and 2 μm of membrane. Rates also shown on membrane prepared by electroless deposition of gold for 0.25 hours versus POM concentration (filled squares).

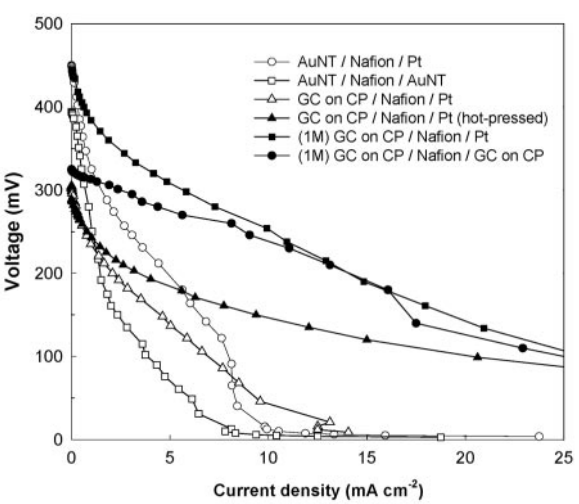

Fig. 3. Voltage-current curves on the various combinations of anodes, membranes, and cathodes with reduced $H_3PMo_{12}O_{40}$ solution used as fuel. As an oxidant, O_2 was used for the Pt cathode and oxidized $H_3PMo_{12}O_{40}$ was used for gold or carbon cathodes. All curves were obtained with 0.5 M $H_3PMo_{12}O_{40}$, except the filled squares and filled circles with 1 M solution. AuNT, gold nanotube membrane deposited for 2 hours with surface gold; Pt, Pt/C cathode; GC, graphitic carbon; CP, carbon paper.

studies demonstrate the feasibility of making new generations of inexpensive fuel cells that operate with solutions of reduced POM compounds and that have current densities of at least 10 mA cm^{-2}. This current density was increased by a factor of 3 at 100 mV and by a factor of 4 or greater at 50 to 100 mV when the assembly consisting of carbon anode, Nafion, and Pt cathode was treated by hot-pressing at 400 K, as included in Fig. 3 (compare open versus filled triangle symbols). Thus, we believe that further optimization with these new fuel cells will lead to improved current densities and improved utilization of precious metals at the electrodes.

References and Notes

1. J. R. Rostrup-Nielsen, T. Rostrup-Nielsen, *CATTECH* **6**, 150 (2002).
2. R. D. Cortright, R. R. Davda, J. A. Dumesic, *Nature* **418**, 964 (2002).
3. G. W. Huber, J. W. Shabaker, J. A. Dumesic, *Science* **300**, 2075 (2003).
4. G. A. Deluga, J. R. Salge, L. D. Schmidt, X. E. Verykios, *Science* **303**, 993 (2004).
5. D. Wang, S. Czernik, E. Chornet, *Energy Fuels* **12**, 19 (1998).
6. Q. Fu, H. Saltsburg, M. Flytzani-Stephanopoulos, *Science* **301**, 935 (2003).
7. N. A. Koryabkina, A. A. Phatak, W. F. Ruettinger, R. J. Farrauto, F. H. Ribeiro, *J. Catal.* **217**, 233 (2003).
8. X. Wang, R. J. Gorte, J. P. Wagner, *J. Catal.* **212**, 225 (2002).
9. C. V. Ovesen *et al.*, *J. Catal.* **158**, 170 (1996).
10. B. C. H. Steele, A. Heinzel, *Nature* **414**, 345 (2001).
11. M. Haruta, T. Kobayashi, H. Sano, N. Yamada, *Chem. Lett.* **2**, 405 (1987).
12. M. Valden, X. Lai, D. W. Goodman, *Science* **281**, 1647 (1998).
13. G. C. Bond, D. T. Thompson, *Gold Bull.* **33**, 41 (2000).
14. M. A. Sanchez-Castillo, C. Couto, W. B. Kim, J. A. Dumesic, *Angew. Chem. Int. Ed. Engl.* **43**, 1140 (2004).
15. S. K. Desai, M. Neurock, *Phys. Rev. B* **68**, 075420 (2003).
16. R. R. Davda, J. A. Dumesic, *Angew. Chem. Int. Ed. Engl.* **42**, 4068 (2003).
17. M. Daté, M. Okumura, S. Tsubota, M. Haruta, *Angew. Chem. Int. Ed. Engl.* **43**, 2129 (2004).
18. H. H. Kung, M. C. Kung, C. K. Costello, *J. Catal.* **216**, 425 (2003).
19. G. M. Brown, M.-R. Noe-Spirlet, W. R. Busing, H. A. Levy, *Acta Crystallogr.* **B33**, 1038 (1977).
20. P. Gómez-Romero, N. Casañ-Pastor, *J. Phys. Chem.* **100**, 12448 (1996).
21. Materials and methods are available as supporting material on *Science* Online.
22. S. Yu, N. Li, J. Wharton, C. R. Martin, *Nano Lett.* **3**, 815 (2003).
23. H. Sakurai, A. Ueda, T. Kobayashi, M. Haruta, *Chem. Commun.*, **1997**, 271 (1997).
24. M. M. Schubert, A. Venugopal, M. J. Kahlich, V. Plzak, R. J. Behm, *J. Catal.* **222**, 32 (2004).
25. L. E. Briand, G. T. Baronetti, H. J. Thomas, *Appl. Catal. A* **256**, 37 (2003).

26. Supported by the National Science Foundation, Daimler-Chrysler, and the U.S. Department of Energy. Fellowships were provided by the Camille and Henry Dreyfus Foundation, the Korea Science and Engineering Foundation, and the Graduate Engineering Scholars program. We thank the Wisconsin Center for Applied Microelectronics for providing facilities; the World Gold Council for providing gold catalysts; P. F. Nealey, T. F. Kuech, S. H. Langer, R. D. Cortright, and M. Mavrikakis for valuable discussions; G. W. Huber for the ethylene glycol experiment; and S. T. Evans, R. Gounder, and C. Couto for assistance in experiments.

Supporting Online Material

www.sciencemag.org/cgi/content/full/305/5688/1280/DC1
Materials and Methods
Figs. S1 and S2
Table S1

28 May 2004; accepted 22 July 2004

Plasminogen Is a Critical Host Pathogenicity Factor for Group A Streptococcal Infection

Hongmin Sun,[1] Ulrika Ringdahl,[6] Jonathon W. Homeister,[2] William P. Fay,[1] N. Cary Engleberg,[1,3] Angela Y. Yang,[4] Laura S. Rozek,[1] Xixi Wang,[1] Ulf Sjöbring,[6] David Ginsburg[1,4,5]*

Group A streptococci, a common human pathogen, secrete streptokinase, which activates the host's blood clot–dissolving protein, plasminogen. Streptokinase is highly specific for human plasminogen, exhibiting little or no activity against other mammalian species, including mouse. Here, a transgene expressing human plasminogen markedly increased mortality in mice infected with streptococci, and this susceptibility was dependent on bacterial streptokinase expression. Thus, streptokinase is a key pathogenicity factor and the primary determinant of host species specificity for group A streptococcal infection. In addition, local fibrin clot formation may be implicated in host defense against microbial pathogens.

Plasmin, the major serine protease that degrades the fibrin blood clot, is generated through cleavage of the proenzyme plasminogen (PLG) by the plasminogen activators urokinase (uPA) and tissue-type plasminogen activator (tPA). Human PLG can also be activated by streptokinase (SK) secreted by group A streptococci (GAS), leading to the clinical use of SK for therapeutic fibrinolysis of pathologic thrombi associated with myocardial infarction, stroke, and venous thrombosis (*1*). PLG deficiency results in the rare genetic disorder ligneous conjunctivitis, characterized by thick fibrinous pseudomembranous deposits on the conjunctiva and other mucous membranes (*2*). PLG null mice develop spontaneous fibrin deposition in multiple tissues, leading to retarded growth, rectal prolapse, and decreased survival (*3*, *4*). *Plg* null mice also exhibit eye findings similar to those for the human disease (*5*). In addition to GAS, a number of other human pathogens also express a plasminogen activator, including staphylokinase of *Staphylococcus aureus* (*6*) and the Pla protein of *Yersinia pestis*, the agent responsible for the plague (*7*). Other microbes, such as *Borrelia burgdorferi*, use a host plasminogen activator as a pathogenicity factor (*8*, *9*). GAS is the most common cause of clinically significant bacterial pharyngeal and skin infections. A subset of these infections are highly invasive into soft tissues or organs and result in rapidly progressive, life-threatening conditions, such as necrotizing fasciitis (*10*). Like many microbial pathogens, GAS is highly host-specific and naturally only infects humans. This restricted host specificity is correlated with the limited ability of many candidate pathogenicity factors, including SK and surface receptors for PLG, to interact with ligands or protein substrates from species other than humans (*11*–*16*). Studies of streptococcal pathogenicity and the role of SK and surface-bound PLG-binding proteins have been hampered by this limitation, as well as by species-specificity in the interactions among host fibrinolytic system components, including tPA and PLG (*17*).

We generated a "humanized" transgenic mouse expressing human PLG under control of the mouse albumin gene regulatory sequences within a bacteria artificial chromosome (BAC) transgene [(*18*) and fig. S1A]. Two independent founder lines, *AlbPLG1* and *AlbPLG2*, directed highly liver-specific *PLG* expression (fig. S1B). The level of PLG detected in the plasma of *AlbPLG1* corresponded to ~17% of the PLG level in control human plasma (16.7 ± 1.78) with a much lower level (<1%) for *AlbPGL2*. Consistent with previous reports (*11*, *15*), human PLG derived from the transgene also exhibited increased susceptibility to activation by human tPA and SK compared with mouse PLG (fig. S1, C and D) (*17*, *19*).

Mice that are $Plg^{-/-}$ are viable but exhibit

[1]Department of Internal Medicine, [2]Department of Pathology, [3]Department of Microbiology and Immunology, [4]Department of Human Genetics, University of Michigan, Ann Arbor, MI 48109, USA. [5]Howard Hughes Medical Institute, Ann Arbor, MI 48109, USA. [6]Department of Laboratory Medicine, Section for Microbiology, Immunology, and Glycobiology, Lund University, SE-221-84 Lund, Sweden.

*To whom correspondence should be addressed. E-mail: ginsburg@umich.edu